


Optical image reconstruction in $4f$ imaging system: Role of spatial coherence structure engineering

Cite as: Appl. Phys. Lett. **118**, 181102 (2021); <https://doi.org/10.1063/5.0046288>

Submitted: 02 February 2021 . Accepted: 17 April 2021 . Published Online: 04 May 2021

Yuechen Shen, Hu Sun, Deming Peng,  Yahong Chen, Qilin Cai, Dan Wu, Fei Wang, Yangjian Cai, and Sergey A. Ponomarenko



View Online



Export Citation



CrossMark

ARTICLES YOU MAY BE INTERESTED IN

Optoelectronic intelligence

Applied Physics Letters **118**, 160501 (2021); <https://doi.org/10.1063/5.0040567>

Epitaxial lift-off CdTe/MgCdTe double heterostructures for thin-film and flexible solar cells applications

Applied Physics Letters **118**, 181101 (2021); <https://doi.org/10.1063/5.0049377>

Curvature-driven homogeneous Dzyaloshinskii–Moriya interaction and emergent weak ferromagnetism in anisotropic antiferromagnetic spin chains

Applied Physics Letters **118**, 182405 (2021); <https://doi.org/10.1063/5.0048823>



David Daughton, PhD
Applications Scientist
Lake Shore Cryotronics

Houston Fortney
Development Engineer
Lake Shore Cryotronics

Mixed AC and DC signals

WEBINAR
A New Concept in Semiconductor Material/Device Characterization
Combining DC and AC Sourcing and Measuring

Watch Now

Lake Shore CRYOTRONICS

Optical image reconstruction in $4f$ imaging system: Role of spatial coherence structure engineering

Cite as: Appl. Phys. Lett. **118**, 181102 (2021); doi: 10.1063/5.0046288

Submitted: 2 February 2021 · Accepted: 17 April 2021 ·

Published Online: 4 May 2021



Yuechen Shen,¹ Hu Sun,¹ Deming Peng,¹ Yahong Chen,^{1,a)}  Qilin Cai,^{1,2,a)} Dan Wu,^{1,3,a)} Fei Wang,^{1,a)} Yangjian Cai,^{1,4,a)} and Sergey A. Ponomarenko^{5,6}

AFFILIATIONS

¹Wenzheng College of Soochow University and School of Physical Science and Technology, Soochow University, Suzhou 215006, China

²School of Rail Transportation, Soochow University, Suzhou 215006, China

³School of Optoelectronic Science and Engineering, Soochow University, Suzhou 215006, China

⁴Shandong Provincial Engineering and Technical Center of Light Manipulations and Shandong Provincial Key Laboratory of Optics and Photonic Device, School of Physics and Electronics, Shandong Normal University, Jinan 250014, China

⁵Department of Electrical and Computer Engineering, Dalhousie University, Halifax, Nova Scotia B3J 2X4, Canada

⁶Department of Physics and Atmospheric Science, Dalhousie University, Halifax, Nova Scotia B3H 4R2, Canada

^{a)}Authors to whom correspondence should be addressed: yahongchen@suda.edu.cn; qlcai@suda.edu.cn; wud@suda.edu.cn; fwang@suda.edu.cn; and yangjiancai@suda.edu.cn

ABSTRACT

We examine the effect of spatial coherence on the image quality of a classic $4f$ imaging system when its Fourier plane is partially blocked by an opaque obstacle. We find that although reducing the degree of spatial coherence of the source results in the improved image quality, the concurrent distortions in the image plane are inevitable. Employing a suitable decomposition of a partially coherent light source into a set of coherent pseudo-modes with a multitude of linear phase shifts, we demonstrate that the distortions are primarily induced by the modes whose maxima are located at the obstacle edges. We show that by tailoring spatial coherence of the source we can enable all the coherent modes to circumnavigate the obstacle, ensuring the same image quality as if the obstacle were absent from the Fourier plane. We expect our findings to be instrumental in high-contrast optical microscopy with coherence structured light.

Published under an exclusive license by AIP Publishing. <https://doi.org/10.1063/5.0046288>

Spatial coherence is among the salient metrics of light, governing many intriguing optical phenomena and featuring in a number of applications.^{1,2} For instance, even a straightforward adjustment of the spatial coherence width of a light source can help reduce the turbulence induced signal distortion in free-space optical communications.^{3,4} Moreover, the spatial coherence distribution of an optical field at the source can be customized to enable a host of applications, such as partially coherent diffractive imaging,⁵ coherence holography,^{6,7} or photovoltaics.⁸ It has been demonstrated recently that a partially coherent beam with tailored spatial coherence structure can self-reconstruct its intensity and polarization upon scattering from an opaque obstacle, provided the spatial coherence length of the beam is relatively low.^{9–12} The physics behind this phenomenon is quite different from that of the self-healing of coherent beams.^{13–15} The self-reconstruction of partially coherent beams can find applications to optical trapping¹⁶ and ghost imaging¹⁷ in random environments.

In this Letter, we explore the effect of spatial coherence on the reconstruction of optical image in a classic $4f$ imaging system when its Fourier plane is partially blocked by an opaque obstacle. It has been well documented to date that low-coherence light illumination in the system results in high-quality images due to the absence of speckles.¹⁸ However, when an obstacle is introduced into the Fourier plane to (partially) block light transmission, distortions inevitably arise in the image plane even for low-coherence light illumination. Here, we employ a suitable coherent pseudo-mode representation^{19,20} of the illuminating source to demonstrate that the just mentioned distortions originate from the source pseudo-modes whose maxima are located at the edge of the obstacle. Our findings indicate the way to engineer the spatial coherence structure of the light source to ensure that all the coherent modes circumnavigate the obstacle, thereby guaranteeing the same image quality as if the obstacle were absent from the system. Since optical microscopy entails a similar $4f$ imaging system, our

results carry promise for high-contrast microscopy with coherence structured light.

We sketch the imaging system employed in our experiment in Fig. 1(a). In Part A, we exhibit the illuminating (partially coherent) light beam generation, while in Part B, we display a classic $4f$ imaging system featuring a pair of thin lenses (L_3 and L_4). We first produce a partially coherent Gaussian Schell model (GSM) beam²¹ with the cross-spectral density

$$W(\mathbf{r}_1, \mathbf{r}_2) \propto \exp\left(-\frac{\mathbf{r}_1^2 + \mathbf{r}_2^2}{4\sigma_0^2}\right) \exp\left[-\frac{(\mathbf{r}_1 - \mathbf{r}_2)^2}{2\delta_0^2}\right],$$

where $\mathbf{r}_1 \equiv (x_1, y_1)$ and $\mathbf{r}_2 \equiv (x_2, y_2)$ are two arbitrary spatial position vectors in the source plane, and σ_0 and δ_0 denote transverse beam intensity and spatial coherence widths, respectively. Here σ_0 is fixed by the aperture of a Gaussian amplitude filter (GAF) which we set at 5 mm in our experiment. At the same time, δ_0 is governed by the size of the beam spot on the rotating ground-glass disk (RGGD), viz., $\delta_0 = \lambda f / \pi w_0$, where $\lambda = 632.8$ nm is the carrier wavelength of the beam, $f = 400$ mm is a focal length of any thin lens of the system, and w_0 is a beam spot size at RGGD. In our experiment, δ_0 varies from 0.1 to 1 mm. The particulars of the GSM beam generation and diagnostics can be found, for instance, in Refs. 22 and 23.

The generated GSM beam illuminates the object plane of the $4f$ imaging system of Fig. 1(a), where we place a 1951 USAF resolution test chart. We place an opaque obstacle into the Fourier plane of the system to partially block the incoming light. For simplicity, we employ

an opaque obstacle shaped as a sector with its opening central angle $\varphi = \pi/4$. We then place a beam profile analyzer (BPA) in the rear focal plane of L_4 to record the output image. We also examine imaging with a fully coherent Gaussian beam of the same width as the GSM beam for comparison. In Fig. 1(b)–1(d), we show the experimental results of the output images generated by an illuminating fully coherent Gaussian beam as well as by the GSM beams with $\delta_0 = 1$ mm and 0.1 mm. The top row of Fig. 1(b)–1(d) shows the results with no obstacle present in the Fourier plane of the system, while the bottom row illustrates imaging with an obstacle.

We can infer from Fig. 1(b)–1(d) that the presence of obstacles obviously degrades the image quality. Moreover, as expected, the speckles inevitably present in the high-coherence illumination case additionally degrade the image as compared to that in the low-coherence illumination case.¹⁸ In fact, the images formed with a high-coherence illumination source [Fig. 1(b) and 1(c)] are badly distorted and fine features are hardly identifiable when the Fourier plane of the system is partially blocked. At the same time, some fine details of the image can be discerned when the same obstacle is present in the low-coherence illumination scenario [Fig. 1(d)]. Yet, image distortions are ubiquitous whenever the Fourier plane of the $4f$ system is even partially blocked.

To better understand how the spatial coherence of the illuminating source affects image quality, we employ a generic pseudo-mode decomposition (PMD) approach of Ref. 19. Unlike the modes of a conventional coherent-mode representation (CMD)²¹ of a partially coherent source, the pseudo-modes do not form an orthogonal set and

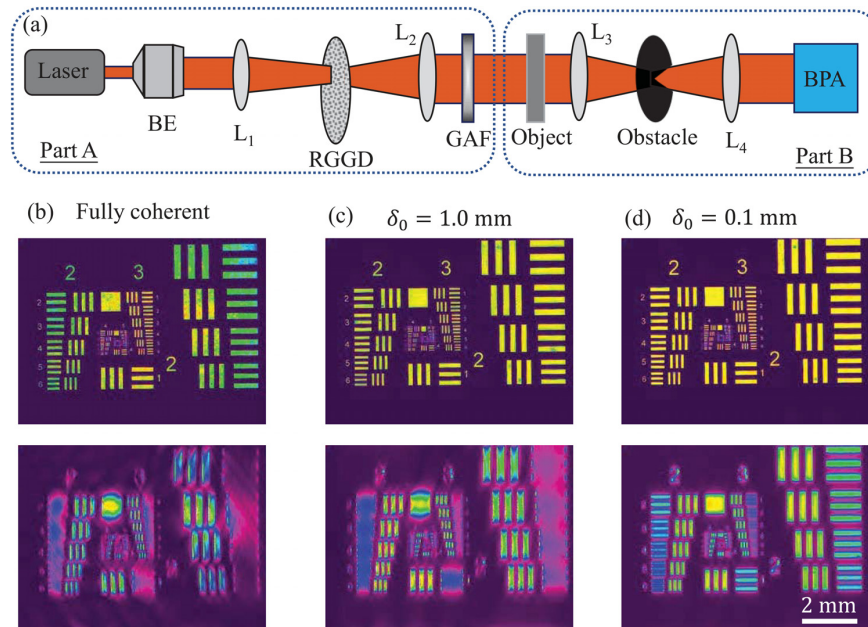


FIG. 1. (a) Schematics of the experimental setup for preparing a GSM beam and the setup for a $4f$ optical imaging system with its Fourier plane partially blocked by a sector-shaped opaque obstacle. (b)–(d) Experimental results of the images of an object illuminated by the light from a fully coherent source (b) and the partially coherent GSM sources [(c) and (d)]. Top panels of (b)–(d) correspond to obstacle free imaging, while bottom panels correspond to the case of an obstructed Fourier plane.

all modes entering the PMD are amplitude- and/or phase-shifted replicas of each other. A particular case of such a PMD, a complex Gaussian representation where the pseudo-modes form an over-complete set of Gaussian beams with a multitude of lateral displacements of beam maxima and linear phase shifts,²⁴ has proven instrumental in studying partially coherent sources.^{25–28} With the help of the PMD, we can reduce the imaging problem at hand to imaging of an individual pseudo-mode. The generic PMD reads¹⁹

$$W(\mathbf{r}_1, \mathbf{r}_2) = \iint p(\mathbf{v}) H^*(\mathbf{r}_1, \mathbf{v}) H(\mathbf{r}_2, \mathbf{v}) d^2\mathbf{v}, \quad (1)$$

where $p(\mathbf{v})$ is a non-negative function for any vector $\mathbf{v} \equiv (v_x, v_y)$ and $H(\mathbf{r}, \mathbf{v})$ is an arbitrary kernel function. For a statistically homogeneous source, the kernel function can be expressed as

$$H(\mathbf{r}, \mathbf{v}) = \sqrt{S(\mathbf{r})} \exp(i2\pi\mathbf{r} \cdot \mathbf{v}), \quad (2)$$

where $S(\mathbf{r}) = W(\mathbf{r}, \mathbf{r})$ is a spectral density of the source. The non-negative function $p(\mathbf{v})$ can then be obtained by

$$p(\mathbf{v}) = \iint \mu(\Delta\mathbf{r}) \exp(-i2\pi\Delta\mathbf{r} \cdot \mathbf{v}) d^2\Delta\mathbf{r}, \quad (3)$$

where $\mu(\Delta\mathbf{r}) = W(\mathbf{r}_1, \mathbf{r}_2) / \sqrt{S(\mathbf{r}_1)S(\mathbf{r}_2)}$ denotes the degree of spatial coherence of the source with $\Delta\mathbf{r} = \mathbf{r}_1 - \mathbf{r}_2$. It is evident from Eq. (3) that $p(\mathbf{v})$ and $\mu(\Delta\mathbf{r})$ form a Fourier transform pair.

To assess a continuous distribution $p(\mathbf{v})$ in the laboratory, we approximate $p(\mathbf{v})$ by a discrete set $\{p_{mn}\}$ of weights at sampled points $\{\mathbf{v}_{mn}\} = \{(v_{xm}, v_{ym})\}$, assuming, for the moment, the sampling functions to be infinitely sharp, such that

$$p(\mathbf{v}) \simeq \sum_{m=0}^{M-1} \sum_{n=0}^{N-1} p_{mn} \delta(\mathbf{v} - \mathbf{v}_{mn}). \quad (4)$$

Here $m = 0, 2, \dots, M-1$ and $n = 0, 2, \dots, N-1$; M and N being the numbers of sampling points along the v_x and v_y axes, respectively. We note that in reality the sampling functions do, of course, have a finite spatial spread; we shall return to this point later in our discussion of the quality of experimentally realized images.

Next, the rank of an M by N sampling matrix depends on a specific distribution $p(\mathbf{v})$. For example, for a GSM source, $p(\mathbf{v}) = (2\pi)^{-1/2} \sigma_p^{-1} \exp(-\mathbf{v}^2/2\sigma_p^2)$ is a Gaussian with the rms width $\sigma_p = 1/(2\pi\delta_0)$ for which we can safely assume that $|v_{xm}| \leq v_{x\max} = 3\sigma_p$ and $|v_{ym}| \leq v_{y\max} = 3\sigma_p$. We notice that the range of phase shifts \mathbf{v}_{mn} is inversely proportional to the spatial coherence width δ_0 of the source, which is directly relevant to the following analysis. It then follows from Eqs. (1) and (4) that

$$W(\mathbf{r}_1, \mathbf{r}_2) \simeq \sum_{m=0}^{M-1} \sum_{n=0}^{N-1} p_{mn} \Phi_{mn}^*(\mathbf{r}_1) \Phi_{mn}(\mathbf{r}_2), \quad (5)$$

where $\Phi_{mn}(\mathbf{r}) = H(\mathbf{r}, \mathbf{v}_{mn})$. Equation (5) represents an experimentally assessable PMD of a partially coherent light source comprised of the pseudo-modes $\{\Phi_{mn}(\mathbf{r})\}$ with a set of weights $\{p_{mn}\}$.

For the Schell-model sources, the pseudo-modes are expressed as

$$\Phi_{mn}(\mathbf{r}) = \sqrt{S(\mathbf{r})} \exp(i2\pi\mathbf{r} \cdot \mathbf{v}_{mn}). \quad (6)$$

We notice that each mode is a phase-shifted, by the amount $\mathbf{v}_{m,n}$, replica of the “ground” mode with the spatial distribution $S(\mathbf{r})$ corresponding to $m = n = 0$. Similarly to the CMD, as the source coherence decreases, the number of modes in the PMD increases, resulting in a broader range of \mathbf{v}_{mn} . In our case, we find that 10^4 modes (i.e., $M = N = 100$) are sufficient to faithfully reproduce the GSM source in the coherence range corresponding to $0.1 \leq \delta_0 \leq 1$ mm.

With the aid of the above PMD, the imaging under the GSM source illumination reduces to the imaging problem for individual pseudo-modes. For a mode of order (m, n) propagating through the $4f$ imaging system, the optical field in the rear focal plane of the first thin lens can be expressed as¹⁸

$$\Psi_{mn}(\mathbf{s}) = \frac{-i}{\lambda f} \iint O(\mathbf{r}) \Phi_{mn}(\mathbf{r}) \exp\left[-i\frac{2\pi}{\lambda f} \mathbf{r} \cdot \mathbf{s}\right] d^2\mathbf{r}. \quad (7)$$

Here $\mathbf{s} \equiv (s_x, s_y)$ is a position vector in the Fourier plane and $O(\mathbf{r})$ is an object transmission function. We assume that an opaque obstacle with a transmission function $t(\mathbf{s})$ is placed in the Fourier plane to partially block the light field. Here we note that a pupil function of the lens¹⁸ is also incorporated into $t(\mathbf{s})$. Therefore, the transmitted light field past the obstacle can be expressed as $t(\mathbf{s})\Psi_{mn}(\mathbf{s})$. After having been transmitted through the second thin lens of the imaging system, the light field in the image plane reads

$$\Phi_{mn}^{\text{image}}(\boldsymbol{\rho}) = \frac{-i}{\lambda f} \iint t(\mathbf{s}) \Psi_{mn}(\mathbf{s}) \exp\left[-i\frac{2\pi}{\lambda f} \mathbf{s} \cdot \boldsymbol{\rho}\right] d^2\mathbf{s}, \quad (8)$$

where $\boldsymbol{\rho} \equiv (x, y)$ is a transverse position vector in the image plane. The integrals in Eqs. (7) and (8) can be evaluated numerically by a fast Fourier transform algorithm. We find for the image intensity: $I_{mn}^{\text{image}}(\boldsymbol{\rho}) = |O(-\boldsymbol{\rho})|^2 S(-\boldsymbol{\rho}) \simeq |O(-\boldsymbol{\rho})|^2$, assuming an ideal imaging system (i.e., $t(\mathbf{s}) = 1$) and illuminating light of nearly uniform intensity. However, as the object transmission function $t(\mathbf{s})$ is not uniform, $t(\mathbf{s}) = 1$ holds only for the area of the Fourier plane outside the obstacle.

We now discuss the reasons for improved image quality with low-coherence light illumination and for the ubiquity of distortions in the image plane. It follows at once on substituting from Eq. (6) into Eq. (7) that

$$\Psi_{mn}(\mathbf{s}) = \Psi_{00}(\mathbf{s} - \lambda f \mathbf{v}_{mn}), \quad (9)$$

where Ψ_{00} stands for the ground mode profile in the Fourier plane; $\mathbf{v}_{00} = 0$ by definition. Further, assuming the maximum of the illuminating light intensity coincides with the optical axis of the system, we can infer that the ground mode maximum lies on the axis of the Fourier plane, $\mathbf{s} = 0$, which coincides with the optical axis. Equation (9) then implies that the intensity maxima of all the other modes are shifted away from the optical axis by $\lambda f \mathbf{v}_{mn}$. Thus, the modes located outside the area blocked by the obstacle are perfectly imaged, whereas those situated within the area are completely blocked by the obstacle. By the same token, the modes with the maxima located at the edges of the obstacle have their images distorted to the point that some fine features are completely blurred. The locations of the mode maxima are governed by the magnitude of \mathbf{v}_{mn} . As an illustration, we depict in Fig. 2 our simulation results for the intensity distributions of a single illuminating pseudo-mode for two pairs of phase shifts \mathbf{v}_{mn} in the Fourier plane as well as the corresponding images of the object in the

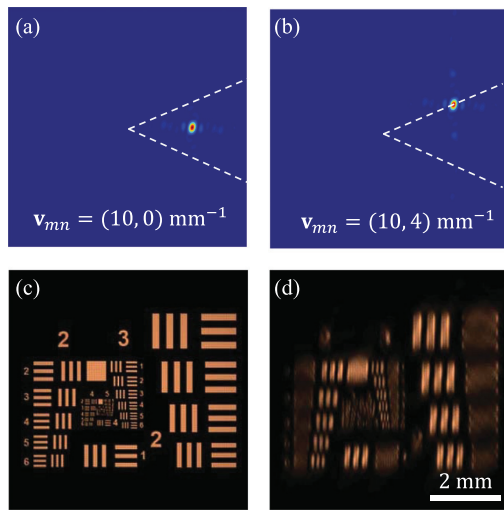


FIG. 2. Simulation results for the intensity distributions of a single pseudo-mode of a GSM source with the phase shift corresponding to $\mathbf{v}_{mn} = (10, 0) \text{ mm}^{-1}$ (left) and $\mathbf{v}_{mn} = (10, 4) \text{ mm}^{-1}$ (right) in the Fourier plane (top) and in the image plane (bottom) of the $4f$ imaging system. The white dashed lines in (a) and (b) represent the edges of the obstacle in the Fourier plane.

image plane. We can infer that for $\mathbf{v}_{mn} = (10, 0) \text{ mm}^{-1}$, the illuminating mode is located entirely inside the opening of the sector-shaped obstacle [Fig. 2(a)], and hence the object is perfectly imaged [Fig. 2(c)]. In the case of $\mathbf{v}_{mn} = (10, 4) \text{ mm}^{-1}$, however, the mode maximum is located at the obstacle edge [Fig. 2(b)], causing pronounced image distortions [Fig. 2(d)].

Let us recall that any realistic set of sampling functions of $p(\mathbf{v})$ must have finite spatial widths Δv_x and Δv_y which determine the required number of sampling points along each of the two mutually orthogonal directions, and hence the effective number of pseudo-modes entering the PMD of any given source. In particular, $M = v_{x\text{max}}/\Delta v_x$ and $N = v_{y\text{max}}/\Delta v_y$, where $v_{x\text{max}}$ and $v_{y\text{max}}$ are the magnitudes of the maximal phase shifts of the modes along the v_x and v_y axes. As $v_{x\text{max}}$ and $v_{y\text{max}}$ are inversely proportional to the coherence width of the source, the number $M \times N$ of the modes required to faithfully reproduce the source increases as the source coherence is reduced. Hence, a greater number of modes falls into the unobstructed area of the Fourier plane illuminated by a source of lower coherence than is the case for imaging with a more coherent source, leading to a greater image quality in the former case compared to the latter. We note that a particular shape of sampling functions does not qualitatively affect the just presented conclusions. In our simulations, we opt for the simplest case of uniform sampling with rectangular sampling functions of widths Δv_x and Δv_y and heights Δv_x^{-1} and Δv_y^{-1} along the corresponding axes. The resulting spatial distribution of the image takes the form

$$S^{\text{image}}(\rho) \simeq \sum_{m=0}^{M-1} \sum_{n=0}^{N-1} p_{mn} |\Phi_{mn}^{\text{image}}(\rho)|^2. \quad (10)$$

We are now in a position to test our theoretical considerations using GSM sources with $\delta_0 = 1.0 \text{ mm}$ and 0.1 mm . We display the

corresponding theoretical $p(\mathbf{v})$ functions in the top panel of Fig. 3. In the bottom panel of Fig. 3, we show the simulation results for the intensity distributions of the images produced by our $4f$ imaging system with a partially blocked Fourier plane. The simulation results clearly show that the image quality improves as the spatial coherence of the source is reduced, which is consistent with our experimental observations and theoretical predictions. However, we also notice image distortions, present regardless of the state of coherence of the illuminating light source, which are known to be caused by the modes on the obstacle edges [see Fig. 2(b) and 2(d)].

To further improve image quality, we can reduce the contribution of the modes located at the obstacle edges by modifying the $p(\mathbf{v})$ function. It follows at once from Eq. (3) that $p(\mathbf{v})$ is governed by the spatial coherence of the source. We can then engineer the coherence structure to ensure that as many modes as possible fall into the unobstructed area of the Fourier plane. We illustrate this point using a Laguerre-Gaussian Schell model (LGSM) source for which²³ $p(\mathbf{v}) = (\pi^{2l+1} \delta_0^{2l+2} 2^{l+1}/l!) \mathbf{v}^{2l} \exp(-2\pi^2 \delta_0^2 \mathbf{v}^2)$,²³ where l is the order of a Laguerre polynomial. We exhibit the distributions of $p(\mathbf{v})$ with $l=2$ and 5 in Fig. 4(a) and 4(d), respectively. The spatial coherence width δ_0 in both cases equals to 0.1 mm , the same as that of the GSM source of Fig. 3. The simulation results in Fig. 4(b) and 4(e), as well as the experimental results in Fig. 4(c) and 4(f), confirm the image quality improvement as the GSM source is replaced with the LGSM one of the same coherence width. However, since the majority of the modes are still completely blocked by the obstacle, as is evident from Fig. 4(a) and 4(d), the transmitted light intensity is very low, yielding low contrast images due to a low signal-to-noise ratio (SNR) [see Fig. 4(c) and 4(f)].

To produce high quality and high SNR images, we propose to tailor the spatial coherence structure of the illuminating source to an obstacle shape. As the obstacle has a sector-shaped opening in our case, $p(\mathbf{v})$ can be modified to fit inside the sector shown in Fig. 5(a) with white dashed lines, which enables all the source modes to

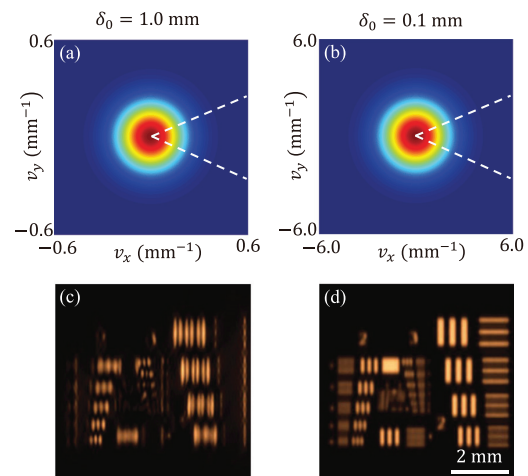


FIG. 3. Simulation results for the distributions of $p(\mathbf{v})$ (top) and image intensity (bottom) with the GSM illuminating light source of spatial coherence width $\delta_0 = 1.0 \text{ mm}$ (left) and 0.1 mm (right).

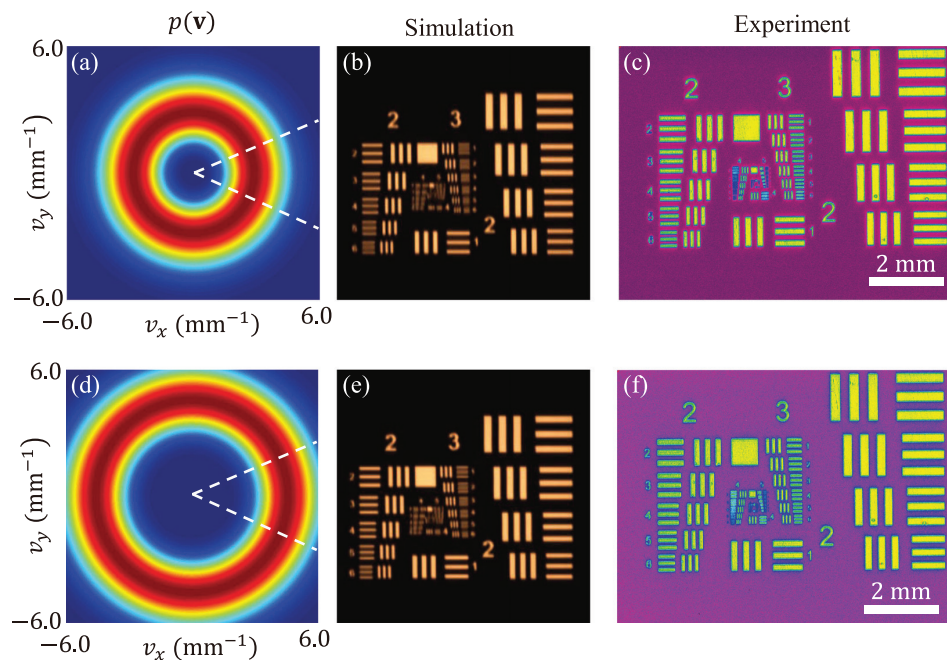


FIG. 4. Simulation results for the distribution of $p(\mathbf{v})$ corresponding an LGSM illuminating source of order (a) $l=2$ and (d) $l=5$. The results of simulations [(b) and (e)], and experiments [(c) and (f)], for the images produced by the $4f$ imaging system illuminated by the LGSM sources of orders $l=2$ and $l=5$.

circumnavigate the obstacle. It follows that $t(s) = 1$ holds for all the source modes which augurs well for the image quality. Once the desired profile of $p(\mathbf{v})$ has been determined, the degree of spatial coherence of the illuminating Schell-model source can be inferred

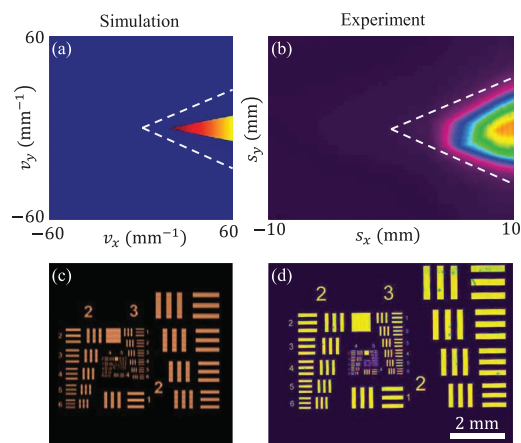


FIG. 5. (a) Spatial distribution of the tailored $p(\mathbf{v})$ function and (c) the corresponding simulation results for the image generated by the $4f$ imaging system. Experimental results for the intensity distributions in the Fourier plane (b) and in the image plane (d) of the system.

from Eq. (3) and realized in experiment via a generalized van Cittert–Zernike method.²³ The results of our simulations and experiments, exhibited in Fig. 5(c) and 5(d), respectively, demonstrate the same (excellent) quality of the image as though the Fourier plane of our imaging system were unencumbered by any obstacle.

In summary, we examined the role of the spatial coherence of the illuminating light source in optical imaging in a classic $4f$ imaging system with its Fourier plane partially blocked by an opaque obstacle. We have shown that as the spatial coherence of the source decreases, the image quality improves although the image distortions are always present. We have coached the imaging problem in terms a pseudo-mode decomposition of the illuminating light source into a set of mutually uncorrelated modes. We have found that the image distortions can be interpreted in terms of some source modes having their maxima located at the edges of the obstacle. We have then explained how engineering the spatial coherence structure of illuminating light can enable these modes to circumnavigate the obstacle leading to high-contrast images of the same quality as if the obstacle were absent. We expect that the elucidated role of optical coherence structuring in image processing can be instrumental in a multitude of applications, e.g., to high-contrast optical microscopy.

This work was supported by the National Key Research and Development Project of China (No. 2019YFA0705000), the National Natural Science Foundation of China (NSFC) (Nos. 11525418, 91750201, 11874046, 11904247, and 11974218), the Innovation Group of Jinan (No. 2018GXRC010), the China

Postdoctoral Science Foundation (No. 2019M661915), the Innovation and Entrepreneurship Training Program for College Students in Jiangsu Province (No. 201913983004Y), the Natural Sciences and Engineering Research Council of Canada (No. RGPIN-2018-05497), and the Local Science and Technology Development Project of the Central Government (No. YDZX20203700001766).

DATA AVAILABILITY

The data that support the findings of this study are available from the corresponding authors upon reasonable request.

REFERENCES

- ¹O. Korotkova and G. Gbur, *Prog. Opt.* **65**, 43 (2020).
- ²Y. Chen, A. Norrman, S. A. Ponomarenko, and A. T. Friberg, *Prog. Opt.* **65**, 105 (2020).
- ³J. C. Ricklin and F. M. Davidson, *J. Opt. Soc. Am. A* **19**, 1794 (2002).
- ⁴J. C. Ricklin and F. M. Davidson, *J. Opt. Soc. Am. A* **20**, 856 (2003).
- ⁵X. Lu, Y. Shao, C. Zhao, S. Konijnenberg, X. Zhu, Y. Tang, Y. Cai, and H. Urbach, *Adv. Photonics* **1**, 016005 (2019).
- ⁶Z. Huang, Y. Chen, F. Wang, S. A. Ponomarenko, and Y. Cai, *Phys. Rev. Appl.* **13**, 044042 (2020).
- ⁷Z. Dong, Z. Huang, Y. Chen, F. Wang, and Y. Cai, *Opt. Express* **28**, 20634 (2020).
- ⁸S. Divitt and L. Novotny, *Optica* **2**, 95 (2015).
- ⁹F. Wang, Y. Chen, X. Liu, Y. Cai, and S. A. Ponomarenko, *Opt. Express* **24**, 23735 (2016).
- ¹⁰X. Liu, X. Peng, L. Liu, G. Wu, C. Zhao, F. Wang, and Y. Cai, *Appl. Phys. Lett.* **110**, 181104 (2017).
- ¹¹G. Wu and X. Pang, *IEEE Photonics J.* **9**, 1 (2017).
- ¹²Z. Xu, X. Liu, Y. Chen, F. Wang, L. Liu, Y. E. Monfared, S. A. Ponomarenko, Y. Cai, and C. Liang, *Opt. Express* **28**, 2828 (2020).
- ¹³P. Fischer, H. Little, R. L. Smith, C. Lopez-Mariscal, C. T. A. Brown, W. Sibbett, and K. Dholakia, *J. Opt. A* **8**, 477 (2006).
- ¹⁴J. Broky, G. A. Siviloglou, A. Dogariu, and D. N. Christodoulides, *Opt. Express* **16**, 12880 (2008).
- ¹⁵Z. Bouchal, *Opt. Commun.* **210**, 155 (2002).
- ¹⁶G. Wu, M. Zhou, Y. Zhou, and Y. Cai, *J. Quant. Spectrosc. Radiat. Transfer* **224**, 171 (2019).
- ¹⁷Y. Zhou, G. Wu, Y. Cai, F. Wang, and B. J. Hoenders, *Appl. Phys. Lett.* **117**, 171104 (2020).
- ¹⁸J. W. Goodman, *Statistical Optics* (John Wiley & Sons, 1985).
- ¹⁹F. Gori and M. Santarsiero, *Opt. Lett.* **32**, 3531 (2007).
- ²⁰R. Martínez-Herrero, P. M. Mejías, and F. Gori, *Opt. Lett.* **34**, 1399 (2009).
- ²¹L. Mandel and E. Wolf, *Optical Coherence and Quantum Optics* (Cambridge University, 1995).
- ²²Y. Cai, Y. Chen, J. Yu, X. Liu, and L. Liu, *Prog. Opt.* **62**, 157 (2017).
- ²³Y. Cai, Y. Chen, and F. Wang, *J. Opt. Soc. Am. A* **31**, 2083 (2014).
- ²⁴S. A. Ponomarenko, *Opt. Express* **19**, 17086 (2011).
- ²⁵L. Ma and S. A. Ponomarenko, *Opt. Lett.* **39**, 6656 (2014).
- ²⁶L. Ma and S. A. Ponomarenko, *Opt. Express* **23**, 1848 (2015).
- ²⁷Y. Chen, S. A. Ponomarenko, and Y. Cai, *Sci. Rep.* **7**, 39957 (2017).
- ²⁸H. Mao, Y. Chen, C. Liang, L. Chen, Y. Cai, and S. A. Ponomarenko, *Opt. Express* **27**, 14353 (2019).